Reaction rates in classical chaotic ABC molecules

1995 J. Phys. A: Math. Gen. 28 2481

(http://iopscience.iop.org/0305-4470/28/9/011)

J. Phys. A: Math. Gen. 28 (1995) 2481–2497. Printed in the UK

Reaction rates in classical chaotic ABC molecules

B Bruhn

Fachbereich Physik, Ernst-Moritz-Arndt Universität, Domstrasse 10a, D-17489 Greifswald, Germany

Received 28 July 1994, in final form 26 January 1995

Abstract. We investigate the reaction rates in a classical chaotic model of ABC triatomics by means of analytical and numerical methods. There are different contributions to the reactive flux depending upon the parameters of the molecule and the total energy, respectively. For small coupling the cantorus flux dominates, whereas for a larger coupling parameter the lobe and turnstile dynamics near the unperturbed separatrix become important. A measure of the ratio of the reactive flux for the reaction and the backreaction, respectively, is discussed. The basic assumption for the derivation of this measure is the existence of a compound state of the molecule. Good agreement between numerical calculations and analytical predictions has been found.

1. Introduction

The basic assumption of the classical theory of reaction rates is that the reacting system can be described by the motion of a representative point in the phase space of the system [1]. The phase space is then divided by a trial surface into regions corresponding to the reactants and the products, and the rate can be calculated approximately by means of the flux through this surface.

On the other hand, the present investigations of simple dynamical systems with few degrees of freedom have shown that the motion of representative points in the phase space can be a very complicated matter. In the case that the dynamics are partly or wholly chaotic, the boundary which divides the reactants from the products may not be smooth. Indeed, the *natural* boundaries between chaotic regions have a Cantor-type structure. These natural boundaries are formed by the stable and unstable manifolds of hyperbolic sets of the associated Poincaré map. Moreover, one can use these invariant manifolds to precisely define partial barriers between different regions in phase space. The determination of the flux across the partial barriers is the main problem of the theory of transport and therefore it is also the main problem of the calculation of reaction rates in a classical system. The flux is determined by measuring the turnstile lobe area [2], however, this measurement will be a complicated problem in the case that there are different types of partial barriers in the phase space, e.g. cantori and broken separatrices.

In two recent papers [3, 4] we have studied a near-integrable system, where cantori, elliptic periodic orbits, transverse homoclinic and transverse heteroclinic orbits occur. Similar systems have been studied in chemical physics in [5–8] (see also the references in [3, 4] for similar systems in other fields of physics). The coexistence of qualitatively different regions in the phase space gives rise to different contributions to the effective reactive flux. For example, in the region of bounded solutions the cantori are the main barriers, whereas

0305-4470/95/092481+17$19.50

near the borderline of bounded and unbounded solutions the broken separatrix plays an important role. Additional difficulties arise from the dependence of the flux upon the actual parameters and the total energy of the system.

In this paper we investigate the classical stretching dynamics of ABC triatomics which are modelled by two coupled Morse oscillators (see also [4]). A special effort is made to study the reactive flux by means of numerical and analytical methods. In section 2 we introduce the equations of motion of the underlying model. Moreover, this section contains a numerical study of the reactive flux and a comparison with theoretical predictions. In section 3 we discuss a first step toward the determination of the equilibrium rate constants of the corresponding chemical reaction starting from the dynamics of the single molecule. An analytical formula for the ratio of the reactive flux of the reaction and the backreaction, respectively, is derived. The basic assumption for the derivation is the existence of a compound state of the molecule and our numerical experiments show that this assumption is justified, at least in a certain range of the parameter space. The existence of such an intermediate collision complex has also been observed in numerical experiments for unimolecular reactions some years ago [9], however, the use of the Melnikov method provides an analytical tool to find approximations for the reactive flux across the perturbed invariant manifolds. In section 4 we summerize our results and conclusions. In appendix A some elementary scaling transformations of the basic equations are discussed. The scaling map is helpful because it links the dynamical and geometrical quantities in both scattering channels. In appendix B selected formulae are listed which describe the critical parameters for channel transitions.

2. Basic equations and numerical determination of reaction rates

In [4] we have investigated the classical stretching dynamics of ABC triatomics in a simplified model. The system is defined by the dimensionless Hamiltonian function

$$H(y_1, y_2, x_1, x_2) = \tfrac{1}{2}(y_1^2 + y_2^2) - \varepsilon y_1 y_2 + D(\mathrm{e}^{-Ax_1} - 1)^2 + (\mathrm{e}^{-x_2} - 1)^2 \tag{2.1}$$

where x_1 and x_2 are the radial position coordinates which describe the deviation from the equilibrium distance between AB and BC, respectively, and y_1 and y_2 are the canonically conjugate momenta. The parameters ε, A and D are related to the molecule parameters by

$$\varepsilon = \frac{\cos\theta}{\sqrt{\left(1+\frac{m_B}{m_A}\right)\left(1+\frac{m_B}{m_C}\right)}} \qquad D = \frac{D_1}{D_2}$$
$$A = \frac{A_2}{A_1}\sqrt{\frac{m_C(m_B+m_C)}{m_A(m_B+m_A)}} \tag{2.2}$$

where θ is the fixed bending angle; m_A, m_B and m_C are the masses of the atoms concerned and D_1 and D_2 are the dissociation energies of the AB and BC binding, respectively. A_1 and A_2 describe the range of the potential which is modelled by two Morse-type functions. The corresponding equations of motion then read

$$\begin{aligned} \dot{x}_1 &= y_1 - \varepsilon y_2 & \dot{y}_1 &= 2AD(\mathrm{e}^{-Ax_1} - 1)\mathrm{e}^{-Ax_1} \\ \dot{x}_2 &= y_2 - \varepsilon y_1 & \dot{y}_2 &= 2(\mathrm{e}^{-x_2} - 1)\mathrm{e}^{-x_2}\,. \end{aligned} \tag{2.3}$$

We will restrict our considerations to the case of small values of ε because in that case the methods of perturbation theory become applicable. This case is realized for masses

$m_B \gg m_A, m_C$. For $\varepsilon = 0$ the equations of motion split into two independent Morse oscillators, where the energy functions

$$H_1 = \tfrac{1}{2}y_1^2 + D(e^{-Ax_1} - 1)^2 = E_1 \qquad H_2 = \tfrac{1}{2}y_2^2 + (e^{-x_2} - 1)^2 = E_2 \tag{2.4}$$

of the single oscillators are constants of motion. Of course, then the phase space of the system has the structure of a direct product of the two single phase spaces and the solutions can be found from the well known solution of the single Morse oscillator. In order to study the behaviour of the system for $\varepsilon \neq 0$, we fix two surfaces of section by

$$\Sigma_1 = \{(x_1, y_1) \mid x_2 = 0, y_2 > 0\} \tag{2.5}$$

$$\Sigma_2 = \{(x_2, y_2) \mid x_1 = 0, y_1 > 0\} \tag{2.6}$$

and consider the Poincaré map $P : \Sigma_i \to \Sigma_i$ $(i = 1, 2)$ induced by the solutions of the equations of motion (2.3). Of course, a variation of the total energy E yields different internal motion types of the molecule. For $E < \min(1, D)$ bounded solutions can be found only, whereas for $E > D + 1$ all three atoms can be free. The intermediate interval $\max(1, D) < E < D + 1$ is the most interesting one because bounded and unbounded solutions are possible and the system can be considered as a two-channel scattering system. The asymptotic limit of the scattering is the limit $x_1 \to \infty$ (channel 1) or $x_2 \to \infty$ (channel 2). The motion within these channels can be described on the corresponding surfaces of section Σ_1 or Σ_2. Of course, there is no smooth crossing between these two surfaces, however, other global sections (cf the discussion in [3]) also show some discontinuities. Moreover, the occurrence of discontinuities in the Poincaré map seems to be a general property in two degrees of freedom Hamiltonian systems with a non-trivial energy surface [10]. Figure 1 shows the Poincaré section Σ_1 for selected initial values and parameters $E = 1.5$, $A = 0.8$, $D = 1.3$ and $\varepsilon = 0.01$. We observe stable periodic orbits ($m = 1, 2, 3$) whose loci are marked by some nearby secondary KAM tori. The unstable periodic orbits and their chaotic neighbourhood are not shown here. Between the $m = 1$ and the $m = 2$ resonances we find a primary KAM torus. On the other hand, we observe the main stochastic layer for all initial conditions which are sufficiently close to the transverse

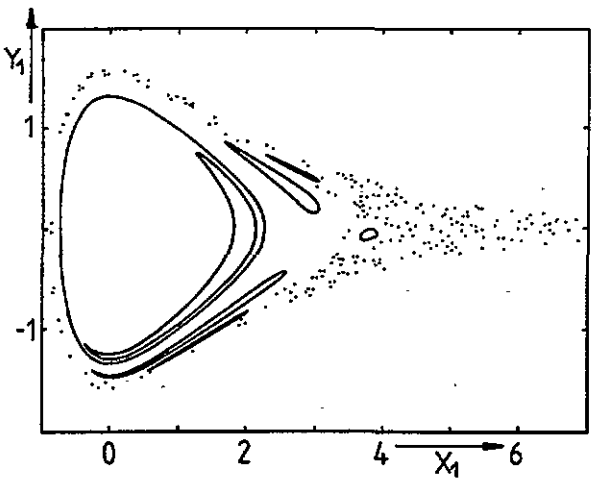

Figure 1. Poincaré section plot Σ_1 for selected initial values and parameters: $E = 1.5$, $A = 0.8$, $D = 1.3$ and $\varepsilon = 0.01$.

homoclinic orbit which is connected with the fixed point at infinity. Additional details of the phase space structure of the system can be found in [3, 4].

The calculation of reaction rates which are based on the dynamics of the single molecule is one of the basic problems in chemical physics. Next we discuss some numerical experiments in order to study the qualitative behaviour of the reaction rate for the single molecule. Of course, a chemical reaction takes place if there are channel transitions of a scattering trajectory and one observes an intramolecular energy flow from one of the atoms to the other. In order to find the reaction rate, one has to fix a set of initial data in the asymptotic range (channel 1 or 2) of the potential. The evolution of this set can be studied by means of a numerical integration of (2.3) and one expects that some parts of the initial set make a channel transition and some other parts lead to simple backscattering. Moreover, some exceptional initial points correspond to trajectories which remain within a bounded region of the potential for all times. Then the reaction rate can be found by the relative abundance N/N_0 of the number of channel transitions N for a large number N_0 of initial points.

In order to obtain comparable results for all values of the parameters A and D, the asymptotic region is fixed in channel 2 by $x_2 \geqslant 40$ because the equation of subsystem 2 does not contain any parameter. The asymptotic region in channel 1 is determined by the condition that the forces $\dot{y}_1$ and $\dot{y}_2$ have the same numerical value, i.e. by using of (2.3) we obtain in the limit of large x_1 and x_2

$$x_1 = -\frac{1}{A} \ln\left(\frac{\exp(-x_2)}{AD}\right). \tag{2.7}$$

Therefore the asymptotic region in channel 1 depends on the asymptotic value x_2 as well as on the actual parameters A and D. We fix the momentum of the second oscillator at $y_2 = 0$ for initial values in the channel 1. The energy conservation then yields the following relationship between x_2 and y_1:

$$x_2 = -\ln\left(1 \pm \sqrt{E - D - \tfrac{1}{2}y_1^2}\right). \tag{2.8}$$

Hence, the momentum y_1 is restricted to the interval

$$y_1 \in \left[-\sqrt{2(E-D)}, \sqrt{2(E-D)}\right]$$

and the set of incoming asymptotes can be labelled by

$$y_1^{in} = y_1 \in [-\sqrt{2(E-D)}, 0). \tag{2.9}$$

We chooe a uniform distributed number N_y of points (a typical value of N_y is 1000 or 2000) in the entire interval (2.9). In order to exclude some effects which arise from the special value of the asymptotic initial points x_1 and x_2, an averaging is performed over a set of $N_x = 20$ different sections in the asymptotic interval $x_2 \in [40, 45]$. Therefore the total number of initial points amounts to $N_0 = N_x N_y$.

Figure 2 shows a typical numerical result of the dependence of the reaction rate upon the coupling parameter ε. The corresponding initial data are chosen in channel 1 and, of course, the rate depends upon the other parameters as shown by the two curves for $A = 0.5$ and $A = 2.0$. In the case of very small values of ε the rate is zero and this indicates the existence of a primary KAM torus which forms a complete barrier between the two channels. Orbits cannot intersect this invariant surface and are confined in the first channel. The scattering is chaotic, however, it is a simple backscattering. Above a critical threshold value the rate increases with increasing coupling parameter. The dependence seems to be approximately described by a linear function over a large range. This observation suggests that the main contribution to the reactive flux comes from the turnstile lobe dynamics near the unperturbed

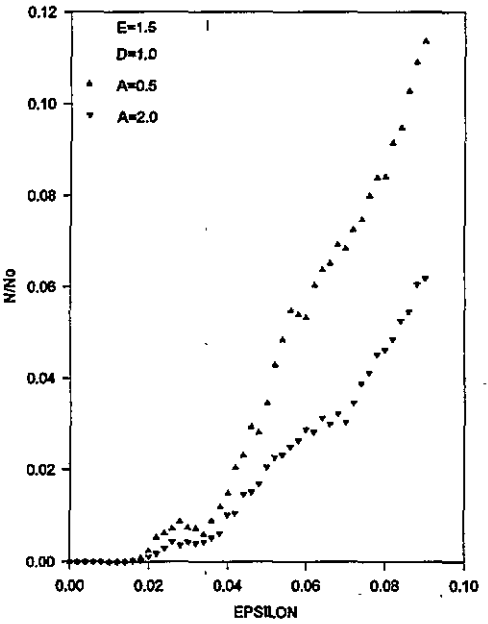

Figure 2. Dependence of the reaction rate N/N_0 upon ε; parameters: $E = 1.5$, $D = 1.0$, $A = 0.5$ and $A = 2.0$. Initial data in channel 1.

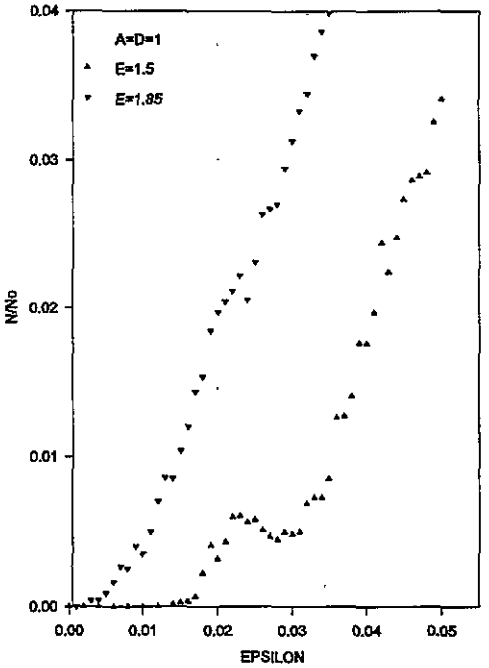

Figure 3. Dependence of the reaction rate N/N_0 upon ε; parameters: $A = D = 1$, $E = 1.5$ and $E = 1.85$.

separatrix because the lobe area is proportional to the coupling ε (cf equation (A.10)). The dependence cannot be described by a linear function near the threshold value. Figure 3 shows this region more precisely in the case of a symmetrical molecule. For $E = 1.5$ we find a local maximum near $\varepsilon \approx 0.023$. The major barriers to transport in this region appear to be the cantori at least for energies E which are not close to $E = D + 1$. Therefore the cantorus flux ΔW_ν restricts the reactive flux between the channels. ΔW_ν is defined by the maximum of the differences in action for minimax orbits in the gaps of the cantorus (cf [16]). Using renormalization theory, a scaling law can be obtained for the cantorus flux ΔW_ν which is expected to be valid for any system provided ε is close enough to the threshold value [14, 15]. The essential dependence is given by

$$\Delta W_\nu \sim \left(\ln\left(\frac{\varepsilon}{\varepsilon_1^c}\right)\right)^\zeta \qquad \zeta \approx 3.0117 \tag{2.10}$$

where $\varepsilon > \varepsilon_1^c$ and ε_1^c is the threshold value which can be calculated by means of (B.3) or (B.4). We have performed a numerical analysis in order to test the universality of the scaling law (2.10) near the breakup also in the case of reactive scattering. Using the same parameters as in figure 3 and $E = 1.5$, a reference point ε_0 is chosen in the interval $0.0125 < \varepsilon_0 < 0.024$. Then the scaling law yields

$$\left(\frac{\Delta W_\nu(\varepsilon)}{\Delta W_\nu(\varepsilon_0)}\right)^{1/\zeta} = \frac{\ln(\varepsilon/\varepsilon_1^c)}{\ln(\varepsilon_0/\varepsilon_1^c)}$$

or by substitution the rate N/N_0 for the flux ΔW_ν

$$\left(\frac{N(\varepsilon)}{N(\varepsilon_0)}\right)^{1/\zeta} = \frac{\ln(\varepsilon/\varepsilon_1^c)}{\ln(\varepsilon_0/\varepsilon_1^c)}$$

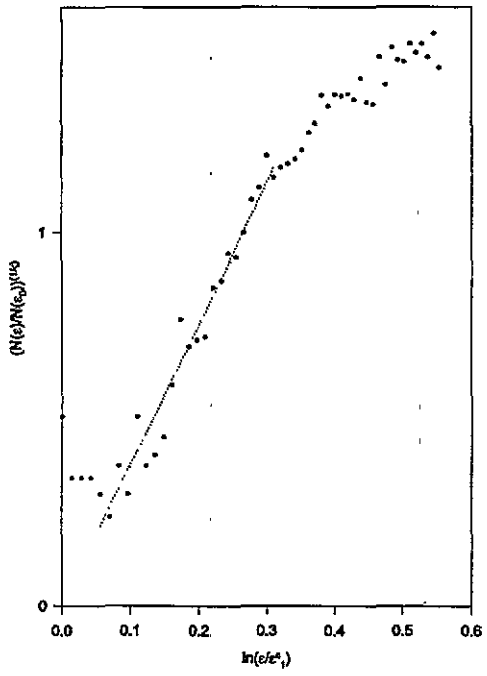

Figure 4. Test of the scaling law near the breakup of invariant tori; parameters: $E = 1.5$, $D = 1.0$, $A = 1.0$, $\varepsilon_0 = 0.018$, $\varepsilon_1^c = 0.0138$, $N_0 = 40\,000$. The dotted line indicates the region of the linear dependence.

Table 1. Comparison of the theoretical and numerical threshold values of the coupling ε for selected parameters.

E	A	D	$\max(\varepsilon_1^r, \varepsilon_2^r)$	$\max(\varepsilon_1^c, \varepsilon_2^c)$	ε_N
1.30	1.0	1.0	0.019	0.016	0.021
1.50	1.0	1.0	0.014	0.009	0.014
1.85	1.0	1.0	0.006	0.001	0.003
1.70	1.0	1.5	0.019	0.015	0.020
2.00	2.0	1.5	0.010	0.013	0.010
2.20	4.0	1.5	0.004	0.009	0.009
1.70	1.5	1.0	0.008	0.005	0.006
1.70	1.5	1.5	0.019	0.026	0.022
2.30	1.5	2.0	0.015	0.017	0.019

i.e. we expect a proportion $(N(\varepsilon))^{1/\zeta} \sim \ln(\varepsilon/\varepsilon_1^c)$. Figure 4 shows the results of the numerical experiment for $\varepsilon_0 = 0.018$ and $\varepsilon_1^c \approx 0.0138$. We note that ε_1^c is the value of the threshold obtained from the resonance overlap criterion (B.1) which is in better agreement with the numerical value than the threshold calculated by means of (B.3) (see also table 1). Of course, the scaling law (2.10) is not valid for larger coupling parameters ε, for example figure 4 shows that for $\varepsilon > 0.019$ ($\ln(\varepsilon/\varepsilon_1^c) > 0.32$) deviations from the linear dependence occur. On the other hand, the statistical error becomes large for $(\varepsilon/\varepsilon_1^c) \to 1$ because the number of channel transitions tends to zero in this limit, however, there is a finite range where the correct behaviour (2.10) can be observed.

The onset of the linear dependence of the rate for larger values of the coupling ε (cf figure 3) seems to be connected with the existence of a transverse heteroclinic orbit. Such orbits appear by intersection of the manifolds of the periodic orbit at

infinity with the manifolds of the symmetric stretching orbit (cf [3]). For $E = 1.5$ the theoretical value $\varepsilon_1^h = 0.0312$ is in quantitative agreement with the beginning of the linear dependence (cf equations (B.5) and (B.6)). For larger values of the energy (see the curve for $E = 1.85$ in figure 3) the linear dependence upon ε dominates over the whole interval. Indeed, the dynamics occur closer to the separatrices and the lobes becomes more important. Moreover, the critical values of the onset of the channel transitions and the value of the onset of heteroclinic intersections are of the same order. For $E = 1.85$ we find by using the overlap condition (cf equation (B.1)) $\varepsilon_1^r = 0.005\,96$ and the corresponding value for heteroclinic intersections amounts to $\varepsilon_1^h = 0.009\,57$. The threshold calculated from (B.3) has the somewhat smaller value $\varepsilon_1^c = 0.001\,13$.

In order to check the quality of the theoretical threshold values of the channel transition, we have performed some numerical scattering experiments for selected values of A, D and E. The results are shown in table 1, where ε_N is the corresponding numerical value which is determined from the first non-vanishing value of the rate. The comparison shows that the theoretical thresholds ε^r and ε^c are of the same order and the differences to the numerical value are rather small, i.e. the theoretical thresholds give a good approximation.

In the last analysis of this section we study the question of whether our numerical quantity N/N_0 is the correct measure to describe the reaction rate or the reactive flux between the two channels. The flux represents a physical action and therefore we expect a scaling law as (A.11) if the scaling transformations of appendix A are performed. The scaling law can be tested by two independent numerical calculations which start in channel 1 and channel 2, respectively. By using parameters in agreement with $A/\sqrt{D} = 1$ and scaling the energy according to (A.4), we expect to obtain the same rate for the reaction and the backreaction, respectively. Figure 5 shows the result of such a numerical experiment and we find a perfect agreement with our expectations.

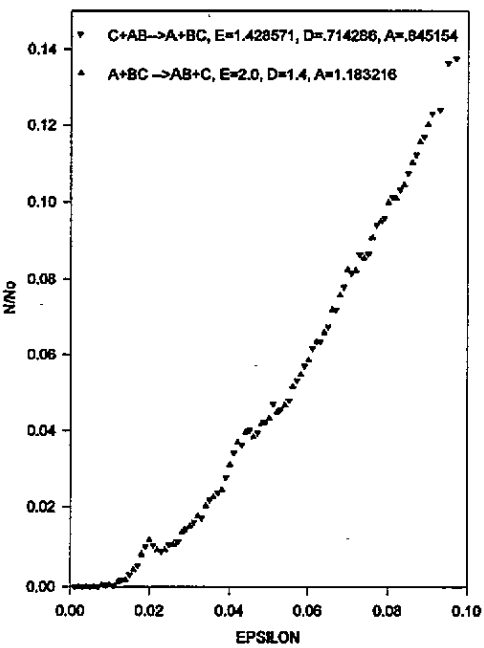

Figure 5. Dependence of the reaction rate N/N_0 upon ε for the reaction and the backreaction, respectively.

3. A measure of the reactive flux rates

Let S_1 be the reactive flux for the reaction

$$A + BC \xrightarrow{k_1} AB + C \tag{3.1}$$

i.e. for the flux from channel 1 into the channel 2 and let S_2 be the corresponding flux for the backreaction

$$AB + C \xrightarrow{k_2} A + BC\,. \tag{3.2}$$

Then the (macroscopic) equilibrium rate constants k_1 and k_2 will depend upon the reactive flux rates S_1 and S_2 of the single molecule. The knowledge of the flux S_1 and S_2 as a function of the total energy E of the molecule opens the possibility of calculating the rate constants by averaging with an equilibrium distribution function. In order to find an approximation of the reactive flux, we consider the following basic assumption: *the reactive process* $A + BC \rightleftharpoons AB + C$ *runs through a compound state* $(ABC)^*$. This assumption is suggested by observations made in numerical experiments. Many scattering trajectories which start in the asymptotic region spend a long time inside the essential interaction region and run alongside bounded chaotic orbits. The mean time of stay in a finite inner region ($x_1, x_2 < \infty$) of the potential is much larger than the time of stay of a free particle in the same region. Moreover, the coupled Morse system is a chaotic one and therefore the trajectory has forgotten its initial conditions after a small number of iterations of the Poincaré map in the compound state (cf [17] and the references therein). The compound state decays if the trajectories run into one of the channels and leave the inner region of the potential. Then the essential point is that the flux rates into the two channels are determined by the decay rates of the compound state. Hence, we have

$$(ABC)^* \longrightarrow AB + C \qquad (ABC)^* \longrightarrow A + BC\,. \tag{3.3}$$

The decay into the two channels can be considered as a kind of a dissociation process from a bounded region of the phase space (see also [15, 18]).

Now let B be the set of initial conditions of the compound state in the phase space with a fixed total energy $E \in (\max(1, D), D + 1)$. We denote the boundary of B by ∂B and define the following subsets:

$$B_1 = B \cap \Sigma_1 \qquad \partial B_1 = \partial B \cap \Sigma_1$$
$$B_2 = B \cap \Sigma_2 \qquad \partial B_2 = \partial B \cap \Sigma_2$$

where Σ_1 and Σ_2 are given by (2.5) and (2.6). On Σ_i the outer boundary of B_i can be well defined by using the segments of the stable and unstable manifolds of the fixed points at infinity. We choose a primary homoclinic intersection point q and segments of the manifolds which connect the point q with the corresponding fixed point at infinity. It is appropriate to choose this so-called pseudoseparatrix so that it is as close as possible to the separatrix of the associated integrable problem. The conservation of the total energy E of the system then provides the inner boundary of B_i. In order to make this construction more clear, we describe the region of the compound state in terms of the unperturbed system $\varepsilon = 0$. In this case the phase flow has the product structure $\gamma_1(E_1)\gamma_2(E_2)$, where γ_i $(i = 1, 2)$ is one of the periodic solutions of the subsystem i and E_i are the corresponding energies defined by (2.4). The unperturbed separatrices Γ_i are the limiting solutions

$$\Gamma_1 = \lim_{E_1 \to D} \gamma_1(E_1) \qquad \Gamma_2 = \lim_{E_2 \to 1} \gamma_2(E_2)$$

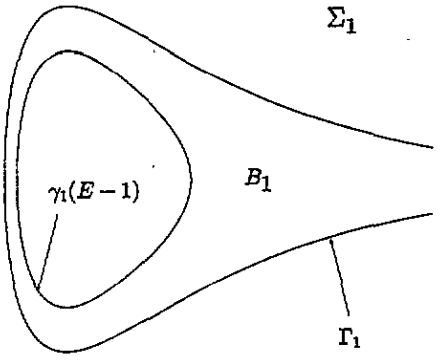

Figure 6. Qualitative structure of the compound region B_1 on the section Σ_1

of the periodic orbits. Taking into account the conservation of the total energy $E = E_1 + E_2$, we have the product flow

$$\gamma_1(E_1)\gamma_2(E - E_1) \tag{3.4}$$

and this will be considered as a one-parameter family (parameter E_1) of solutions for a fixed E. In the limit $E_1 \to D$ we obtain the solution $\Gamma_1\gamma_2(E - D)$. Of course, Γ_1 is the outer boundary of the compound state on Σ_1 and $\gamma_2(E - D)$ is the inner boundary of B_2 on Σ_2. Continuous decrease of E_1 so that $(E - E_1) \to 1$ yields the solution $\gamma_1(E - 1)\Gamma_2$, where now $\gamma_1(E - 1)$ is the inner boundary of B_1 and Γ_2 is the outer boundary of B_2. Therefore the compound region B_1 on Σ_1 has a ring shape bounded by $\partial B_1 = \Gamma_1 \cup \gamma_1(E - 1)$ and on Σ_2 we find the boundary $\partial B_2 = \Gamma_2 \cup \gamma_2(E - D)$. Figure 6 shows the qualitative structure of the compound region on the section Σ_1. This is a rough estimation because one observes islands of order around the elliptic periodic orbits on Σ_i in the perturbed problem $\varepsilon \neq 0$ (cf also figure 1). These regions of order must be subtracted from the compound state because any trajectory which starts within these islands is confined for all times and cannot contribute to the decay rate. Moreover, the coupling parameter ε must be sufficiently large so that all primary KAM tori are destroyed and the trajectory can pass from one resonance to another within the whole compound state. Some of the threshold values are given in the appendix B.

Using the interpretation of the lobe area $\mu(L_i)$ as the instantaneous flux across the unperturbed separatrix, we describe the relative part of the compound state which escapes into the first channel in one step of the map $\Sigma_1 \to \Sigma_1$ by $\mu(L_1)/\mu(B_1)$. The corresponding quantity on Σ_2 is $\mu(L_2)/\mu(B_2)$. More precisely, one has to consider the quotient $\mu(L_i \cap B_i)/\mu(B_i)$ because the lobes may partially intersect the compound region B_i (see our discussion at the end of this section). However, in a first step we consider the simplified version. In order to compare both quantities we have to take into account that the step size is different on Σ_1 and Σ_2, respectively. This can be seen, for example, in the unperturbed solutions $\gamma_1(E - 1)$, $\gamma_2(E - D)$ or by consideration of the two periodic orbits at infinity. Therefore we define the time normalized flux by

$$S_1 = \frac{\mu(L_1)}{\mu(B_1)T(\gamma_2(E - D))} \qquad S_2 = \frac{\mu(L_2)}{\mu(B_2)T(\gamma_1(E - 1))} \tag{3.5}$$

where $T(\gamma_i)$ is the period of the corresponding periodic orbits at infinity. The lobe area on the cross sections can be calculated by means of the homoclinic Melnikov functions up to the first order in ε to give (A.10) and (A.12). Therefore we obtain a first-order result for

the flux S_i by using the unperturbed solutions in the calculation of $\mu(B_i)$ and $T(\gamma_i)$. This analysis is easy to perform and one obtains

$$\mu(B_1) = \oint_{\Gamma_1} y_1 \, dx_1 - \oint_{\gamma_1(E-1)} y_1 \, dx_1 = \frac{2\pi\sqrt{2}\Omega}{A}$$

$$\mu(B_2) = \oint_{\Gamma_2} y_2 \, dx_2 - \oint_{\gamma_2(E-D)} y_2 \, dx_2 = 2\pi\sqrt{2}\Omega$$

and

$$T(\gamma_1) = \frac{2\pi}{A\sqrt{2}\Omega} \qquad T(\gamma_2) = \frac{2\pi}{\sqrt{2}\Omega}$$

where Ω is defined by (A.7). Using these results and (A.10), (A.12) one finds (3.5) to have the form

$$S_1 = \frac{A}{4\pi^2}\mu(L_1) = \frac{\varepsilon\sqrt{2}\Omega\sqrt{1-\Omega^2}}{\pi\left(\sinh\left(\frac{\Omega}{A\sqrt{D}}\right) + \Omega\cosh\left(\frac{\Omega}{A\sqrt{D}}\right)\right)} \tag{3.6}$$

$$S_2 = \frac{A}{4\pi^2}\mu(L_2) = \frac{\varepsilon\sqrt{2}A\Omega\sqrt{D-\Omega^2}}{\pi\left(\sqrt{D}\sinh(A\Omega) + \Omega\cosh(A\Omega)\right)}. \tag{3.7}$$

Moreover, we define the function $R(E, A, D)$ by

$$R(E, A, D) = \frac{S_2}{S_1} = \frac{\mu(L_2)}{\mu(L_1)} = \frac{A\sqrt{D-\Omega^2}\left(\sinh\left(\frac{\Omega}{A\sqrt{D}}\right) + \Omega\cosh\left(\frac{\Omega}{A\sqrt{D}}\right)\right)}{\sqrt{1-\Omega^2}\left(\sqrt{D}\sinh(A\Omega) + \Omega\cosh(A\Omega)\right)} \tag{3.8}$$

where the dependence upon E results from (A.7). The function R describes the ratio of the decay rates of the compound state. The formation of the compound state can be understood in a similar manner and one finds the same result by using the fact that the inward flux and the outward flux across the unperturbed separatrix have the same value. Hence, the function R must be a measure of the reactive flux rates.

Let us discuss some properties of this function. An application of the scale transformation of appendix A provides the inverse function R^{-1} as it must be if the channels are exchanged. Furthermore, $R(E, A, D)$ is independent on ε at least in the first order of the perturbation theory, however, ε must be larger than the threshold values for channel transitions in order to secure that the reactive flux is non-zero. In the special case of symmetrical molecules $A = D = 1$ one obtains $R = 1$ over the whole range of the total energy. This is correct from the physical point of view because the symmetrical model is invariant with respect to a permutation of the two channels. The dependence upon the parameter A provides

$$\lim_{A\to 0} R(E, A, D) = \infty \qquad \lim_{A\to\infty} R(E, A, D) = 0 \tag{3.9}$$

i.e. one of the flows S_1, S_2 tends to zero, however, the rate of convergence is very different for (3.6) or (3.7). Of course, this is an effect of the integrability of the equations of motion (2.3) in the limit $A \to 0$ or $A \to \infty$. On the other hand, the limit $E \to D + 1$ (or $\Omega \to 0$) yields

$$\lim_{E\to D+1} R(E, A, D) = 1 \tag{3.10}$$

which seems to be evident because for $E > D + 1$ the atoms can move over the whole (x_1, x_2) coordinate space. But it must be underlined that this limit is hard to discuss because

the area of the compound state $\mu(B_i)$ tends to zero. In the case of the unperturbed problem this is compensated by the increasing periods $T(\gamma_i)$ (cf the denominator in (3.5)), but in the perturbed problem one cannot exclude some variations. Moreover, there is a second point of interest which is connected with the decrease of the area of the compound state $\mu(B_i)$. The lobe area is fixed by

$$\lim_{E\to D+1}\mu(L_1)=\lim_{E\to D+1}\mu(L_2)=\frac{\varepsilon 4\pi\sqrt{2}}{\left(A+1/\sqrt{D}\right)} \tag{3.11}$$

and the inner boundaries of B_i tend to the separatrices Γ_i. Therefore the region of intersection of the lobes L_i and of the compound state B_i shrinks to zero, i.e. one expects that only parts of the lobes fall into the compound region B_i. As a matter of principle, our assumption $\mu(L_i\cap B_i)\approx\mu(L_i)$ becomes wrong for values of E coming close to $D+1$. In order to give a simple estimation of the range of the validity of (3.8), we use the maximum of the homoclinic Melnikov function which characterizes the width of the main stochastic layer near the unperturbed separatrix [11]. For $E\to D+1$ we have (cf [4] or appendix B of this paper)

$$\lim_{E\to D+1}\tilde{M}_1=\lim_{E\to D+1}\tilde{M}_2=\frac{9\pi DA}{\sqrt{3}(1+A\sqrt{D})^2} \tag{3.12}$$

where $\tilde{M}_i$ is the maximum of $M_i(t_0)$. Our approximations (3.6) and (3.7) break if on the section Σ_1

$$\varepsilon\tilde{M}_1\approx E_1|_{\Gamma_1}-E_1|_{\gamma_1(E-1)}=D+1-E \tag{3.13}$$

and by using (3.12) one finds the critical energy $E=E^*$ to have the value

$$E^*=D+1-\frac{9\pi\varepsilon DA}{\sqrt{3}(1+A\sqrt{D})^2}. \tag{3.14}$$

Here we have taken into account the interpretation of the maximum $\tilde{M}_i$ as a measure of the width of the main stochastic layer in terms of the unperturbed energy levels. The calculation on Σ_2 yields the same result. It must be noted that we have overestimated $\tilde{M}_i$ by (3.12) because the maximum of the Melnikov function depends upon the total energy E, however, our result (3.14) gives the correct order. For values of the energy $E>E^*$ there is the possibility of defining some effective areas of the lobes which model the area of $\mu(L_i\cap B_i)$, however, this will not be considered in this paper.

We illustrate some properties of our theoretical result (3.8) by numerical experiments. Two sets of initial data as described in section 2 are chosen in channel 1 and channel 2, respectively. The quotient of the rates, i.e. the number of channel transitions into the second channel divided by the number of transitions into the first channel gives the numerical quantity corresponding to the function $R(E, A, D)$. Figure 7 shows the dependence on ε for fixed $E=2$, $D=1.5$, $A=2$ and $A=4$. The dotted lines indicate the theoretical results calculated by means of (3.8). We find statistical fluctuations around the theoretical result and the mean value of the numerical data seems to be independent of ε as predicted by (3.8). Of course, the statistical error becomes large for small ε because, near the threshold value, only very few transitions occur. We hope that the results can be improved by increasing the total number of initial points, however, the problems are permanent near the threshold value of the coupling. The numerical experiment shows that there is a small decay of R for larger values of ε, e.g. for $A=4$ and $\varepsilon=0.3$ we find $R\approx 0.25$. We next consider the dependence of R upon the total energy which is represented in figure 8. Note that for any value of the energy a new interval of initial conditions (cf equation (2.9)) has been used. In the range

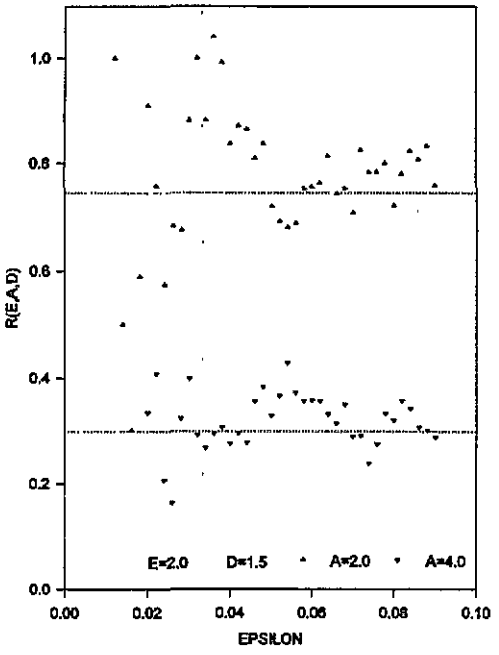

Figure 7. Dependence of the function $R(E, A, D)$ upon ε; parameters: $E = 2.0$, $D = 1.5$, $A = 2.0$ and $A = 4.0$. The dotted lines correspond to (3.8).

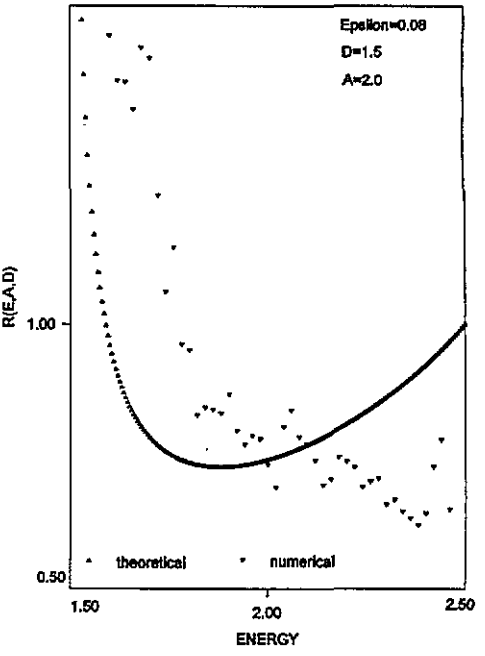

Figure 8. Dependence of $R(E, A, D)$ upon the total energy E; parameters: $\varepsilon = 0.08$, $D = 1.5$ and $A = 2$

$1.5 < E < 2$ the function decreases with increasing energy as predicted by our theoretical result. The difference between the numerical result and the theoretical predictions become large for $E \to 2.5$. Using equation (3.14) we find the associated critical value of the energy $E^* = 2.17$ which gives the boundary of the applicability of (3.8). One may think that the range of the applicability can be extended in the limit $\varepsilon \to 0$ because then E^* tends to $D + 1 = 2.5$ (cf equations (3.14)). However, in this limit the KAM tori becomes important and the reactive flux is zero. It is remarkable that our simple model works at all because the dynamics of the scattering trajectories show a very complicated behaviour in the mentioned interval of the energy. The results of this section can be summarized by the statement that the agreement between the theoretical and numerical results is not perfect, but we can find qualitatively and, at least in some parameter regions, quantitatively correct description of some properties of the reaction rates.

4. Conclusions

In this paper we have shown that the methods of the classical theory of transport, i.e. the dynamics of the lobes and turnstiles can be applied to the coupled Morse system. Our model is in some sense a generic one because the qualitative properties remain the same for other physical potentials. For example, the Lenard–Jones potential provides a similar two-channel model with unstable periodic orbits at infinity. Moreover, one finds transverse intersecting manifolds, chaotic scattering, regions of order near the elliptic periodic orbits and channel transitions which model a chemical reaction. The main difference to the Morse problem is that the analytical calculations of the perturbation theory are more complicated and cannot be performed in all details. However, a numerical analysis of reaction rates is

always possible. The only property of the coupled Morse system which is in some sense non-generic is the absence of the Arnold diffusion which does not occur in problems having less than three degrees of freedom.

In order to make the comparison with the (real) experiment, one has to calculate the equilibrium rate constants starting from (3.6)–(3.8). As a matter of principle, this can be performed by ensemble averaging, i.e. one assumes that the reacting molecules are independent of each other. For a real physical system this condition is equivalent to the statement that the mean free path of the molecule must be large compared with the interaction range and, of course, this is fulfilled for most of gases away from the critical point.

Moreover, molecules are objects which must be described by means of quantum mechanics and therefore our classical model contains some of the limiting properties of real molecules only. The finite value of Planck's constant restricts the localization in the classical phase space and significant channel transitions can be observed only if the reactive flux exceed the value of this constant. The situation is similar to that for multiphoton ionization [15] and the consideration of quantum effects yields an elevation of the classical thresholds. Moreover, it has been shown [19] that some classical properties of transport have a counterpart in quantum spectral fluctuations, i.e. some information of the classical flux can be translated in terms of random matrix theory. On the other hand, there are many open questions concerning the quantum problem and as much knowledge as possible of the underlying classical system may be helpful to clarify some of them.

Acknowledgments

This work was supported by DFG (Deutsche Forschungsgemeinschaft) grant no Ko 1323/2-1. The author would like to thank Dr B P Koch for a number of comments and helpful discussions.

Appendix A.

In reference [4] we have used the methods of perturbation theory to prove the existence of chaotic scattering and of elliptic and hyperbolic periodic orbits, to calculate the width of the main stochastic layer and of resonances and to predict the range of initial conditions where singularities in the scattering function are found. All these quantities are calculated on Σ_1 and can be found by an analogous consideration also on Σ_2. However, there is a very simple map which connects the relevant quantities on Σ_1 with that on Σ_2. In order to find this map we consider the equations of motion (2.3), perform the scale transformation:

$$\begin{aligned} x_1' &= Ax_1 \qquad x_2' = Ax_2 \qquad t' = A\sqrt{D}t \\ y_1' &= y_1/\sqrt{D} \qquad y_2' = y_2/\sqrt{D} \end{aligned} \tag{A.1}$$

and define a new set of parameters by

$$D' = 1/D \qquad A' = 1/A \qquad \varepsilon' = \varepsilon\,. \tag{A.2}$$

Hence, the new equations of motion are given by

$$\begin{aligned} \dot{x}_1' &= y_1' - \varepsilon' y_2' \qquad \dot{y}_1' = 2(\mathrm{e}^{-x_1'} - 1)\mathrm{e}^{-x_1'} \\ \dot{x}_2' &= y_2' - \varepsilon' y_1' \qquad \dot{y}_2' = 2A'D'(\mathrm{e}^{-A'x_2'} - 1)\mathrm{e}^{-A'x_2'} \end{aligned} \tag{A.3}$$

where the overdot indicates the differentiation with respect to the time t'. A comparison with (2.3) shows that the new equations of motion have a similar form but now with the new

parameters (A.2). Additionally the index of channels (or subsystems) has been changed, i.e. the surface of section Σ_1 in favour of (A.3) (defined as (2.5) with a dash) corresponds to the surface Σ_2 for (2.3). Therefore any scattering process which starts in channel 1 with parameters A, D, ε is related to a scattering process which starts in channel 2 with parameter A', D', ε'. Of course, the total energy E must also be transformed. Using (2.1), (A.1) and (A.2) one finds the scaling law

$$E' = \frac{E}{D}. \tag{A.4}$$

The physical meaning of the scaling map becomes clear by consideration of (2.2) because the transformation (A.2) can be realized by the exchange

$$m_A \longleftrightarrow m_C \qquad A_1 \longleftrightarrow A_2 \qquad D_1 \longleftrightarrow D_2$$

i.e. we have permuted the atoms A and C, respectively. It must be underlined that $\varepsilon = \varepsilon'$ is invariant which is important because our results in [3,4] are based on a power series expansion with respect to this parameter. Therefore the order of the perturbation theory is not changed after an application of the scaling transformation.

Now let $f_1(E, A, D, \varepsilon, \ldots)$ be a physical quantity which characterizes the dynamics on Σ_1. Then there is the connection

$$f_1(E, A, D, \varepsilon, \ldots) = \lambda(A', D') f_2(E', A', D', \varepsilon, \ldots) \tag{A.5}$$

where $\lambda(A', D')$ is a scaling factor which results from the dimensional analysis of the function f_1, and $f_2(E, A, D, \varepsilon, \ldots)$ (i.e. without the dash!) is the corresponding function on Σ_2. In order to give an example, we study the homoclinic Melnikov function on Σ_1. This function is given by [4]

$$M_1(t_0) = \frac{4\pi\Omega^2\sqrt{1-\Omega^2}\alpha \sin(\sqrt{2}\Omega t_0)}{A\left(\beta - \sqrt{1-\Omega^2}\cos(\sqrt{2}\Omega t_0)\right)^2} \tag{A.6}$$

where

$$\alpha = \sinh\left(\frac{\Omega}{A\sqrt{D}}\right) + \Omega\cosh\left(\frac{\Omega}{A\sqrt{D}}\right)$$

$$\beta = \cosh\left(\frac{\Omega}{A\sqrt{D}}\right) + \Omega\sinh\left(\frac{\Omega}{A\sqrt{D}}\right)$$

and

$$\Omega = \sqrt{1 + D - E}. \tag{A.7}$$

The Melnikov function is a first-order measure of the distance separating the stable and unstable manifolds of the fixed point at infinity on Σ_1. Simple zeros of this function prove the existence of an invariant hyperbolic set Λ which contains the chaotic orbits [11]. From the physical point of view the product $\varepsilon M_1(t_0)$ represents an energy increment (cf [12]) and we expect a scaling law of the form

$$M_1(t_0; E, A, D) = \frac{1}{D'} M_2(t_0'; E', A', D') \tag{A.8}$$

i.e. the scaling factor $\lambda(A', D')$ is that of the energy (cf equation (A.4)). Inserting (A.1), (A.2) and (A.4) into the function $M_1(t_0; E, A, D)$ provides

$$M_1 = \frac{1}{D'} \frac{4\pi A'\Omega'^2\sqrt{D' - \Omega'^2}\tilde{\alpha}' \sin(\sqrt{2}A'\Omega' t_0')}{\left(\tilde{\beta}' - \sqrt{D' - \Omega'^2}\cos(\sqrt{2}A'\Omega' t_0')\right)^2}.$$

Moreover, the comparison with (A.8) yields

$$M_2(t_0) = \frac{4\pi A\Omega^2\sqrt{D-\Omega^2}\tilde{\alpha}\sin(\sqrt{2}A\Omega t_0)}{\left(\tilde{\beta}-\sqrt{D-\Omega^2}\cos(\sqrt{2}A\Omega t_0)\right)^2} \tag{A.9}$$

where

$$\tilde{\alpha} = \sqrt{D}\sinh(A\Omega) + \Omega\cosh(A\Omega) \qquad \tilde{\beta} = \sqrt{D}\cosh(A\Omega) + \Omega\sinh(A\Omega)\,.$$

The function $M_2(t_0)$ measures the distance between the stable and unstable manifold of the fixed point at infinity on Σ_2. The same result can be obtained by a direct calculation of the homoclinic Melnikov function by means the unperturbed separatrix solution

$$x_2(t,t_0) = \ln\left(\tfrac{1}{2}+(t-t_0)^2\right) \qquad y_2(t,t_0) = \frac{2(t-t_0)}{\frac{1}{2}+(t-t_0)^2}$$

and one of the periodic solutions of the subsystem 1. However, the use of the scaling properties is very simple compared to the direct evaluation of the Melnikov integral.

The turnstile lobe dynamics is the central point of interest for the understanding of the relationship between the phase space geometry and the dynamics in the homoclinic tangle [2, 13]. The partial barriers (e.g. the broken separatrix) and the turnstiles are fixed in the Poincaré map, and the lobe area $\mu(L)$ on the cross section which represents the instantaneous flux across these partial barriers can be approximated by means of the homoclinic Melnikov function according to

$$\mu(L) = \varepsilon\int_{t_{01}}^{t_{02}} |M(t_0)|\,\mathrm{d}t_0 + O(\varepsilon^2)$$

where t_{01} and t_{02} describe two neighbouring zeros of $M(t_0)$. Using (A.6) the calculation is easy to perform and the result on Σ_1 is given by

$$\mu(L_1) = \frac{4\varepsilon\sqrt{2}\pi\Omega\sqrt{1-\Omega^2}}{A\left(\sinh\left(\frac{\Omega}{A\sqrt{D}}\right)+\Omega\cosh\left(\frac{\Omega}{A\sqrt{D}}\right)\right)} \tag{A.10}$$

where Ω is defined by (A.7). In order to find the corresponding formula on Σ_2 an application of the scaling transformation is possible. The lobe area represents a physical action and therefore we expect a scaling law of the form

$$\mu(L_1; E, A, D) = \frac{A'}{\sqrt{D'}}\mu(L_2; E', A', D')\,. \tag{A.11}$$

The simple algebraic calculation provides

$$\mu(L_2) = \frac{4\varepsilon\sqrt{2}\pi\Omega\sqrt{D-\Omega^2}}{\left(\sqrt{D}\sinh(A\Omega)+\Omega\cosh(A\Omega)\right)}\,. \tag{A.12}$$

This result can be calculated, of course, starting from (A.9). Applying the scale transformation in the same manner one can obtain, for example, the threshold values for channel transitions on Σ_2 or some other interesting quantities (cf appendix B).

Appendix B.

In this appendix we list some formulae which can be used to calculate the width of the main stochastic layer, the threshold values for channel transitions and the critical coupling parameters for heteroclinic intersections. The theoretical background and the calculations on Σ_1 can be found in [3, 4] (see also the references therein). In order to find the corresponding

quantities on Σ_2 we have applied the scaling transformations of appendix A, however, the direct evaluation is always possible.

The threshold of breakup of the invariant tori can be calculated by means of the resonance overlap criterion [20]. Let ξ be the function

$$\xi(n,m)=\left(\frac{\sqrt{n^2+m^2A^2}-mA\Omega}{\sqrt{n^2+m^2A^2}+mA\Omega}\right)^{n/2}\left(\frac{\sqrt{D(n^2+m^2A^2)}-n\Omega}{\sqrt{D(n^2+m^2A^2)}+n\Omega}\right)^{m/2}$$

where (m,n) is a pair of integers which characterize the resonance of order m/n. Of course, the threshold value depends upon the order of the resonance, however, we have shown that the $(1,1)$ resonance dominates over a large region of the phase space [4]. Therefore we consider the critical ε of this special resonance only. The value is determined by

$$\sqrt{\varepsilon_1^r}=\frac{3A^{3/2}}{4\sqrt{2}\left((1+A^2)\sqrt{\frac{2\xi(1,2)}{1-\xi^2(1,2)}}+(1+4A^2)\sqrt{\frac{\xi(1,1)}{1-\xi^2(1,1)}}\right)} \tag{B.1}$$

on Σ_1 and, moreover, on Σ_2 one finds

$$\sqrt{\varepsilon_2^r}=\frac{3A^{1/2}}{4\sqrt{2}\left((1+A^2)\sqrt{\frac{2\xi(2,1)}{1-\xi^2(2,1)}}+(4+A^2)\sqrt{\frac{\xi(1,1)}{1-\xi^2(1,1)}}\right)}. \tag{B.2}$$

The onset of channel transitions is determined by the largest value of ε_1^r and ε_2^r, respectively. On the other hand, the threshold value can be calculated by means of the methods of renormalization theory [14, 15]. In this case the $(1,1)$ resonance dominates over the whole interval of A, D and E and the corresponding critical ε are approximately given by

$$\varepsilon_1^c=\frac{R^*(1-\xi(1,1))^3}{2\pi^2A(1+\xi(1,1))\xi(1,1)} \tag{B.3}$$

$$\varepsilon_2^c=\frac{R^*A(1-\xi(1,1))^3}{2\pi^2(1+\xi(1,1))\xi(1,1)} \tag{B.4}$$

where $R^*\approx 0.25008$ is the critical residue. The threshold of channel transitions is determined by $\max(\varepsilon_1^c,\varepsilon_2^c)$ and this is ε_2^c for $A>1$ and ε_1^c for $A<1$.

The simplest possibility of estimating the critical coupling parameters for the existence of transverse heteroclinic orbits in the Morse model has been studied in the case of a symmetrical molecule [3]. This treatment can be generalized to the case $A\neq 1$, $D\neq 1$ by substitution of the $(1,1)$ resonance for the symmetric stretching orbit. We can estimate the critical ε_1^h and ε_2^h by the condition that the energy difference ΔE_i between the unperturbed separatrix solution and the $m=1$, $n=1$ resonance must be filled by the resonance half-width and the half-width of the main stochastic layer. The calculation yields the following estimates:

$$\varepsilon_1^h=\frac{2\Omega^2}{(1+A^2)\tilde{M}_1}\sqrt{\frac{2A\xi(1,1)}{1-\xi^2(1,1)}}\left(-1+\sqrt{1+\frac{\tilde{M}_1(1+A^2)(1-\xi^2(1,1))}{8A\xi(1,1)\Omega^2}}\right) \tag{B.5}$$

$$\varepsilon_2^h=\frac{2A\Omega^2}{(1+A^2)\tilde{M}_2}\sqrt{\frac{2A\xi(1,1)}{1-\xi^2(1,1)}}\left(-1+\sqrt{1+\frac{\tilde{M}_2(1+A^2)(1-\xi^2(1,1))}{8A\xi(1,1)\Omega^2}}\right) \tag{B.6}$$

where the maximum $\tilde{M}_i = \max_{t_0 \in R} M_i(t_0)$ can be calculated by means of the homoclinic Melnikov functions (A.6) and (A.9) to be

$$\tilde{M}_1 = \frac{16\pi\alpha\Omega^2\sqrt{\beta\sqrt{\beta^2+8(1-\Omega^2)}-\beta^2-2(1-\Omega^2)}}{A\sqrt{2}\left(3\beta-\sqrt{\beta^2+8(1-\Omega^2)}\right)^2} \tag{B.7}$$

$$\tilde{M}_2 = \frac{16\pi A\tilde{\alpha}\Omega^2\sqrt{\tilde{\beta}\sqrt{\tilde{\beta}^2+8(D-\Omega^2)}-\tilde{\beta}^2-2(D-\Omega^2)}}{\sqrt{2}\left(3\tilde{\beta}-\sqrt{\tilde{\beta}^2+8(D-\Omega^2)}\right)^2}. \tag{B.8}$$

Here $\alpha, \beta, \tilde{\alpha}, \tilde{\beta}$ and Ω are defined as in appendix A. $\varepsilon\tilde{M}_i$ gives the width of the main stochastic layer on the surface Σ_i in terms of the unperturbed energy levels and the limiting case (3.12) can be found by a discussion of (B.7) and (B.8).

References

[1] Keck J C 1967 Variational theory of reaction rates *Adv. Chem. Phys.* **13** 85–121

[2] Wiggins S 1990 *Introduction to Applied Nonlinear Dynamical Systems and Chaos* (New York: Springer) pp 420–539

[3] Bruhn B and Koch B P 1993 Chaotic scattering in classical triatomic molecular dynamics *Int. J. Bif. Chaos* **3** 999–1012

[4] Koch B P and Bruhn B 1993 Phase space structure and chaotic scattering in near-integrable systems *CHAOS* **3** 443–57

[5] Davis M J 1987 Phase space dynamics of bimolecular reactions and the breakdown of transition state theory *J. Chem. Phys.* **86** 3978–4003

[6] Gray S K, Rice S A and Davis M J 1986 Bottlenecks to unimolecular reactions and an alternative form for classical RRKM theory *J. Phys. Chem.* **90** 3470–82

[7] Gillilan R E and Ezra G S 1991 Transport and turnstiles in multidimensional Hamiltonian mappings for unimolecular fragmentation: application to van der Waals predissociation *J. Chem. Phys.* **94** 2648–68

[8] Zhao M and Rice S A 1992 An approximate classical unimolecular reaction rate theory *J. Chem. Phys.* **96** 6654–65

[9] Davis M J and Gray S K 1986 Unimolecular reactions and phase space bottlenecks *J. Chem. Phys.* **84** 5389–411

[10] de Almeida A M O, de Leon N, Mehta M A and Marston C C 1990 Geometry and dynamics of stable and unstable cylinders in Hamiltonian systems *Physica* **46D** 265–85

[11] Guckenheimer J and Holmes P J 1983 *Nonlinear Oscillations, Dynamical Systems and Bifurcations of Vector Fields* (New York: Springer) pp 184–255

[12] Marsden J E 1992 *Lectures on Mechanics* (Cambridge: Cambridge University Press) pp 207–17

[13] Rom-Kedar V and Wiggins S 1990 Transport in two-dimensional maps *Arch. Rat. Mech. Anal.* **109** 239–98

[14] Greene J M 1979 A method for determing a stochastic transition *J. Math. Phys.* **20** 1183–201

[15] MacKay R S and Meiss J D 1988 Relation between quantum and classical thresholds for multiphoton ionization of excited atoms *Phys. Rev.* A **37** 4702–6

[16] Meiss J D 1992 Symplectic maps, variational principles and transport *Rev. Mod. Phys.* **64** 795–848

[17] Pompe B, Kruscha J and Leven R W 1986 State predictability and information flow in simple chaotic systems *Z. Naturf.* **41a** 801–18

[18] Beigie D and Wiggins S 1992 Dynamics associated with a quasiperiodically forced Morse oscillator: application to molecular dissociation *Phys. Rev.* A **45** 4803–27

[19] Bohigas O, Tomsovic S and Ullmo D 1993 Manifestation of classical phase space structures in quantum mechanics *Phys. Rep.* **223** 43–133

[20] Chirikov B V 1979 A universal instability of many-dimensional oscillator systems *Phys. Rep.* **52** 263–375